PAPER

NJC
www.rsc.org/njc

Solid-state inclusion compounds of small amphiphilic molecules (C_nE_m) in β-cyclodextrin: a study at defined relative humidities

Luís Cunha-Silva* and José J. C. Teixeira-Dias

Department of Chemistry & CICECO, University of Aveiro, Aveiro, P3810-193, Portugal. E-mail: l.m.c.silva@leeds.ac.uk; Fax: +44(0)1133436565; Tel: +44(0)1132336574

Received (in Durham, UK) 23rd May 2005, Accepted 20th July 2005
First published as an Advance Article on the web 2nd August 2005

Solid-inclusion compounds of ethylene glycol butyl ether (C_4E_1), di(ethylene glycol) butyl ether (C_4E_2) and di(ethylene glycol) hexyl ether (C_6E_2) in β-cyclodextrin (βCD), with general formula represented by the notation {βCD · C_nE_m}, were prepared from aqueous solution and characterized by powder X-ray diffraction (PXRD), thermogravimetric analysis (TGA), FT-Raman and ^{13}C CP MAS NMR spectroscopies, at ambient humidity, as true hydrated microcrystalline inclusion compounds, pointing to a cage structure for {βCD · C_4E_1} and a channel structure for both {βCD · C_4E_2} and {βCD · C_6E_2}. In addition, the inclusion compounds were investigated at several defined relative humidities (RHs). Several relative intensities of βCD Raman bands generally ascribed to C–O stretching and CH_2 bending vibrations are found to be influenced by the presence of guests in the βCD cavity or the increase of ambient humidity, or by both of these factors. PXRD patterns show that crystalline structures are preserved for RHs equal or above 20%. Interestingly, important changes on the multiplicity of resonances and in the dispersions of ^{13}C CP MAS NMR chemical shifts values for all the carbon atoms of the βCD macrocycle are observed in passing from RH 15% to 20%, suggesting amorphous structures below RH 20%. Overall, the above findings converge to stress the structural relevance of hydration water in the βCD inclusion compounds, either with a cage packing arrangement or with a channel structure.

Introduction

β-Cyclodextrin (cyclomaltoheptaose, βCD, Fig. 1) is a cyclic oligosaccharide with seven α(1→4) glucopyranose units, resulting in a hollow truncated cone shape. Considering the diversity of OH group environments and of hydration waters included in the cavity and in the interstices between macrocycles, βCD is an important model system to investigate hydration processes, water–biomolecule interactions and non-covalent interactions in biomolecular systems.[1–10]

About seven disordered water molecules are located in each βCD cavity of a βCD crystal in contact with its mother liquor, with five more water molecules in the interstitial sites.[4] Dynamics studies were carried out to investigate disordered hydrogen bonds, exchangeable hydrogen atoms and water molecules of the crystalline βCD hydrates.[11,12] At room temperature, the water molecules contained in the crystal and most of the 21 βCD hydroxyl groups display appreciable positional and/or orientational disorder.[12] Crystal structures were determined for βCD hydrates at various relative humidities (RHs) showing that the hydration water number per cyclodextrin molecule may depend on the crystallization conditions and on the subsequent sample history. While the water content is gradually reduced from 12.3 H_2O (RH = 100%) to about 9.4 H_2O (RH = 15%), the crystal packing arrangement, the pattern of intermolecular hydrogen bonds and the conformation of the βCD molecules are conserved.[4] However, at very low humidities (RH < 15%), the βCD crystalline structure collapses due to loss of hydration water.[6]

Despite its interesting properties as a crystalline hydrate, βCD is better known for its ability to form inclusion compounds, by accommodating guest molecules of suitable size in its cavity.[1,13,14] If the guest displays hydrophobic–hydrophilic behaviour, the βCD cavity has a tendency to host the hydrophobic fragment or part of it, leaving the hydrophilic moiety to interact mainly with hydroxyl groups of βCD.[15,16] When a solid inclusion compound is obtained from an aqueous solution, the resulting crystalline hydrate contains water molecules located in interstitial spaces and in the βCD cavities. It is generally accepted that hydration water has an important role in promoting the stability of inclusion compounds.[17] Despite the large number of investigations which have been carried out on crystalline βCD hydrates, the interactions between hydration water and the βCD macrocycle are not well understood. Moreover, to our knowledge, little attention has been devoted to the influence of hydration water on the stability of the inclusion compounds with guests showing hydrophobic–hydrophilic behaviour.

In previous work we have studied the influence of the relative humidity on the global structure of the solid-state inclusion compounds of 2-phenoxyethanol (PhE_1) and α-*n*-dodecyl-ω-hydroxytetra(oxyethylene) ($C_{12}E_4$) in βCD.[18,19] In this work, particular attention is devoted to the study of solid-state inclusions in βCD of several small amphiphilic molecules of general formula C_nE_m [C_n and E_m stand for $CH_3(CH_2)_{n-1}$– and –$(OCH_2CH_2)_mOH$ moieties, respectively], named α-*n*-alkyl-ω-hydroxyoligo(oxyethylene)s, with different hydrophobic/hydrophilic chain lengths. Crystalline inclusion compounds of C_4E_1, C_4E_2 and C_6E_2 (Fig. 2) in βCD were prepared from aqueous solutions and studied by powder X-ray diffraction (PXRD), thermogravimetric analysis (TGA), vibrational spectroscopy (FTIR and FT-Raman) and ^{13}C CP MAS NMR spectroscopy, at ambient humidity. In addition, to investigate the influence of the hydration level, three solid-state inclusion compounds were studied at several defined RHs (0, 15, 20, 42, 58, 78, 80, 93 and 100%), using PXRD, Raman and ^{13}C CP MAS NMR spectroscopies.

DOI: 10.1039/b507215h

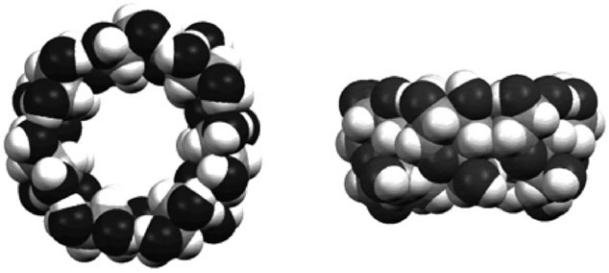

Fig. 1 (βCD) structure: top view (left) and lateral view (right).

Experimental section

Materials and methods

βCD, kindly offered by Wacker-Chemie (Müchen, Germany), was recrystallized from concentrated aqueous solution before use. Ethylene glycol butyl ether (C_4E_1, *Aldrich*, 99%), di(ethylene glycol) butyl ether (C_4E_2, *Aldrich*, 99%) and di(ethylene glycol) hexyl ether (C_6E_2, *Aldrich*, 97%) were used as received. Lithium chloride hydrate ($LiCl \cdot H_2O$, *Riedel-de Haën*, min. 98%), potassium acetate (KCH_3COO, *Riedel-de Haën*, min. 99%), zinc nitrate hexahydrate [$Zn(NO_3)_2 \cdot 6H_2O$, *Fluka*, 99%], sodium bromide ($NaBr \cdot 2H_2O$, *Aldrich*, 99+%), sodium thiosulfate ($Na_2S_2O_3 \cdot 5H_2O$, *Merck*, 99.5%), ammonium chloride (NH_4Cl, *Panreac*, 99.5%) and ammonium dihydrogen phosphate ($NH_4H_2PO_4$, *Panreac*, min. 98%) were used for preparation of saturated salt solutions as received.

FT-Raman spectral studies were carried out on a Bruker RFS 100/S spectrometer, using a Nd/YAG laser line at 1064 μm, with 200–500 mW of power (resolution 1–2 cm^{-1}; 100–2000 scans per spectrum). FTIR spectra were obtained on a Unican Mattson Model 7000 FTIR spectrometer, using KBr pellets (2 cm^{-1} resolution, 32 scans). Room temperature solid-state ^{13}C CP MAS NMR spectra were recorded at 100.62 MHz, on a 9.4 T Bruker Avance 400 spectrometer (25 °C; 3.6 μs ^1H 90° pulses, 2.0 ms contact time, 7–8 kHz spinning rate; 4 s recycle delays). Chemical shifts are quoted in parts per million (ppm) from TMS. Powder XRD data were collected on a Philips X'pert diffractometer using Cu-Kα radiation filtered by Ni (λ = 1.5418 Å). TGA studies were performed on a Mettler TA3000 system, using a heating rate of 1 °C min^{-1}, under nitrogen atmosphere, with a flow rate of 30 mL min^{-1}. The sample holder was a 5 mm ∅ platinum plate and the sample mass was about 5 to 20 mg.

Preparation of inclusion compound

Solid-state inclusion compounds of C_4E_1, C_4E_2 and C_6E_2 in βCD were prepared by the precipitation process. For simplicity, we will hereafter refer to the solid-state inclusion compounds of several C_nE_m in βCD by the shorthand notations {βCD · C_nE_m}. This nomenclature intentionally omits any reference to stoichiometric ratios since these were not determined in this work.

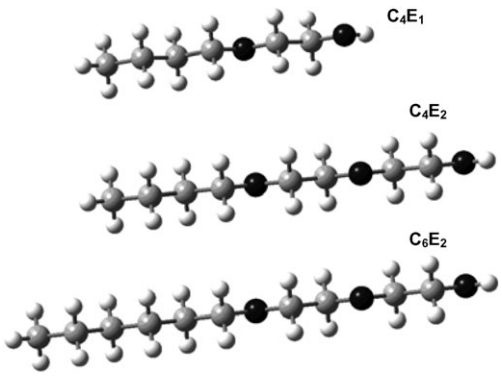

Fig. 2 C_4E_1, C_4E_2 and C_6E_2 structures.

{βCD · C_4E_1} (1). A saturated aqueous solution (2.8 mL H_2O) of βCD (0.493 g, 0.375 mmol) at 70 °C was heated to 80 °C and continuously stirred until complete dissolution of the solid. C_4E_1 (51.9 μL, 0.395 mmol) was added in a stoichiometric proportion and the resulting solution was stirred at *ca.* 80 °C, under reflux, during 24 hours. The reaction mixture was then slowly cooled to room temperature and the obtained white precipitate was filtered, washed with cold distilled water (50 mL), and exposed at room atmosphere for several days. Elemental analysis calcd (%) for $C_{42}H_{70}O_{35} \cdot C_6H_{12}O_2 \cdot 12H_2O$: C 39.24, H 7.42, O 53.35; found (%): C 38.86, H 7.41, O 53.73. ^1H NMR (300 MHz, D_2O, 20 °C, TMS): δ = 4.95–4.94 (d, βCD), 3.87–3.81 (t, βCD), 3.75–3.72 (m, βCD), 3.59–3.40 (m, C_4E_1 and βCD), 1,52–1.45 (m, C_4E_1), 1.38–1.25 (m, C_4E_1), 0.80–0.75 (t, C_4E_1). FTIR (KBr, cm^{-1}): 3374 (vs), 2924 (m), 1647 (w), 1457 (sh, w), 1415 (w), 1382 (w), 1369 (w), 1335 (w), 1304 (w), 1254 (w), 1200 (w), 1158 (s), 1103 (s), 1081 (vs), 1054 (vs), 1030 (vs), 1003 (s), 947 (m), 938 (m), 861 (w), 756 (w), 706 (m), 608 (m), 578 (m), 530 (m). ^{13}C CP MAS NMR: δ = 104.1, 103.6, 103.1, 102.2, 102.0, 101.3 (βCD, C1), 83.7, 83.3, 83.0, 82.2, 81.5, 80.9, 80.4, 80.2, 79.9, 78.2 (βCD, C4), 75.9, 74.7, 74.2, 73.3, 72.7, 72.5, 72.0, 71.2 (βCD, C2,3,5), 63.4, 61.7, 61.0, 59.9 (βCD, C6), 31.6 (C_4E_1, CH_2), 19.2 (C_4E_1, CH_2), 13.7 (C_4E_1, CH_3).

{βCD · C_4E_2} (2). βCD (0.492 g, 0.374 mmol) was dissolved in water (2.9 mL) with heating at 80 °C and continuously stirred until complete dissolution of the solid. C_4E_2 (73.4 μL, 0.437 mmol) was added in stoichiometric and the resulting solution was stirred at *ca.* 80 °C under reflux, during 24 hours. The reaction mixture was slowly cooled to room temperature and the suspension was filtered. The obtained white powder was washed with cold distilled water (50 mL) and exposed at room atmosphere for several days. Elemental analysis calcd (%) for $C_{42}H_{70}O_{35} \cdot C_8H_{18}O_3 \cdot 11H_2O$: C 40.17, H 7.41, O 52.42; found (%): C 40.50, H 7.42, O 52.08. ^1H NMR (300 MHz, D_2O, 20 °C, TMS): δ = 4.95–4.94 (d, βCD), 3.87–3.81 (t, βCD), 3.75–3.72 (m, βCD), 3.62–3.59 (m, C_4E_2), 3.56–3.41 (m, βCD), 1,53–1.46 (m, C_4E_2), 1.37–1.24 (m, C_4E_2), 0.80–0.76 (t, C_4E_2). FTIR (KBr, cm^{-1}): 3355 (vs), 2924 (m), 2877 (sh), 1457 (sh, w), 1430 (w), 1420 (m), 1383 (m), 1371 (m), 1335 (m), 1305 (m), 1249 (m), 1202 (w), 1159 (s), 1101 (s), 1080 (vs), 1056 (vs), 1030 (vs), 1002 (s), 945 (m), 937 (m), 861 (w), 755 (m), 704 (m), 608 (m), 576 (m), 529 (m), 476 (w), 446 (w), 411 (w). ^{13}C CP MAS NMR: δ = 104.0, 103.9, 103.5, 103.0 (βCD, C1), 82.9, 82.5, 82.0, 81.5, 80.9, 80.3, 80.0 (βCD, C4), 74.0, 73.8, 73.3, 73.1, 72.9, 72.5, 72.0, 71.7 (βCD, C2,3,5), 61.4, 61.0, 60.8, 59.9 (βCD, C6), 30.8 (C_4E_2, CH_2), 18.7 (C_4E_2, CH_2), 13.6 (C_4E_2, CH_3).

{βCD · C_6E_2} (3). C_6E_2 (90.9 μL, 0.433 mmol) was added to a stirred solution of βCD (0.495 g, 0.376 mmol) in water (2.9 mL) at 80 °C. This mixture was maintained at this temperature and continuously stirred for 24 hours. The reaction mixture was slowly cooled to room temperature and the suspension was filtered. The obtained white precipitate was washed with cold distilled water (50 mL) and exposed at room atmosphere for several days. Elemental analysis calcd (%) for $C_{42}H_{70}O_{35} \cdot C_{10}H_{22}O_3 \cdot 12H_2O$: C 40.52, H 7.59, O 51.89; found (%): C 40.37, H 7.31, O 52.32. ^1H NMR (300 MHz, D_2O, 20 °C, TMS): δ = 4.95–4.94 (d, βCD), 3.84–3.78 (t, βCD), 3.76–3.62 (m, βCD), 3.59–3.43 (m, C_6E_2 and βCD), 1,50–1.43 (m, C_6E_2), 1.26–1.17 (m, C_6E_2), 0.77–0.72 (t, C_6E_2). FTIR (KBr, cm^{-1}): 3373 (vs), 2924 (m), 1640 (w), 1432 (sh, w), 1414 (m), 1383 (sh, m), 1370 (m), 1334 (m), 1306 (m), 1248 (m), 1203 (w), 1158 (s),

1102 (s), 1081 (vs), 1057 (vs), 1030 (vs), 1003 (s), 945 (m), 937 (m), 862 (w), 755 (m), 703 (m), 575 (m), 530 (m), 476 (w), 446 (w). ^{13}C CP MAS NMR: $\delta = 103.6$ (βCD, C1), 82.4, 82.0, 81.5, 80.9, 80.5, 80.0 (βCD, C4), 74.01, 73.6, 73.1, 72.7, 72.0 (βCD, C2,3,5), 61.2, 60.9, 59.9 (βCD, C6), 31.2, 30,7 (C_6E_2, CH_2), 29.1, 28.7 (C_6E_2, CH_2), 25.8, 25.0 (C_6E_2, CH_2), 22.1 (C_6E_2, CH_2), 13.8 (C_6E_2, CH_3).

Samples at defined RHs

In order to expose the solid-state inclusion compounds at defined RHs, samples were stored during several days (one week at least) in contact with environmental conditions created by silica gel, water and saturated solutions of salts. Defined relative humidities (RHs) were set up by silica gel for RH = 0%, by various saturated salt solutions (RH = 15%, $LiCl \cdot H_2O$; RH = 20%, KCH_3COO; RH = 42%, $Zn(NO_3)_2 \cdot 6H_2O$; RH = 58%, $NaBr \cdot 2H_2O$; RH = 78%, $Na_2S_2O_3 \cdot 5H_2O$; RH = 80%, NH_4Cl; RH = 93%, $NH_4H_2PO_4$), and by pure water for RH = 100%.[4]

Results and discusion

Thermogravimetric analysis (TGA)

Thermal analysis methods can be useful for a quickly indication of host–guest interactions in solid-state inclusion compounds.[20,21] Thermograms for {βCD · C_4E_1}, {βCD · C_4E_2}, {βCD · C_6E_2}, the three corresponding 1 : 1 physical mixtures for comparison, and βCD for reference are presented in Fig. 3.

The thermogram for crystalline βCD is shown in all the parts of the Fig. 3, for clarity. This thermogram shows an initial loss of hydration water up to 80 °C (13.7% mass loss, corresponding to *ca.* 10 hydration water molecules per βCD molecule), with a single inflection point at 76 °C. No further mass change occurs until *ca.* 225 °C when melted βCD starts to decompose as shown by the abrupt mass loss whose differential thermogravimetric (DTA) peak occurs at 285 °C. The TGA results for the three 1 : 1 physical mixtures can all be interpreted in terms of the thermograms of the individual components. The initial step corresponds to the dehydration of βCD, followed by the release (vaporization) of guest molecules [C_4E_1 **(a)**, C_4E_2 **(b)** or C_6E_2 **(c)**]. The last step reflects the decomposition of βCD.

The thermogram of {βCD · C_4E_1} (Fig. 3a) presents an initial mass loss of 3.9% up to 52 °C (inflection point occurs at 49 °C), due to the loss of hydration water. Two additional mass losses of 7.4% (segment line with higher slope, from 52 °C to 83 °C) and 8.1% (segment line with small slope, from 83 °C to 250 °C) should most likely correspond to the release (vaporization) of C_4E_1, following the slow dissociation of {βCD · C_4E_1}. Up to 250 °C, an abrupt loss mass due to decomposition of the melted βCD is observed.

TGA analyses of {βCD · C_4E_2} and {βCD · C_6E_2} (Fig. 3b and 3c, respectively) have similar interpretations to that of the solid-state inclusion compound of C_4E_1 in βCD. Thermograms for both, compounds (**2**) and (**3**), show an initial mass loss (4.9% and 5.9%, respectively) up to 50 °C, ascribed to the dehydration. In addition, {βCD · C_4E_2} and {βCD · C_6E_2} present two mass losses (4.9% between 50 °C and 74 °C, and 7.7% from 74 °C to 250 °C, for compound (**2**); 2.3% between 50 °C and 73 °C, and 9.2% from 73 °C to 250 °C, for compound (**3**)). These mass losses are probably due to the release (vaporization) of guest molecules following the slow dissociation of the solid-state inclusion compounds. The steps ascribed to the loss of hydration water in the {βCD · C_4E_2} and {βCD · C_6E_2} thermograms correspond to smaller mass losses, and occur and end at lower temperatures than for the corresponding steps in the 1 : 1 physical mixtures and in βCD. These thermal features indicate that the hydration water of compounds (**2**) and (**3**) corresponds to a smaller amount of water and is not so strongly bound as in the respective 1 : 1 physical mixtures and βCD, suggesting a channel structure where the water release is easier than in a cage structure.

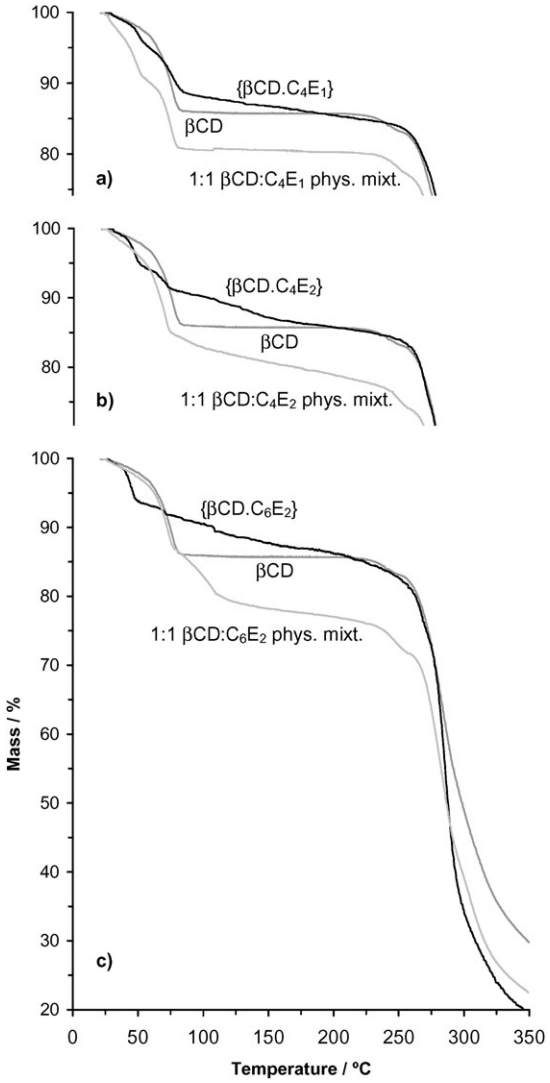

Fig. 3 Thermograms for {βCD · C_4E_1}, 1 : 1 physical mixture of βCD and C_4E_1, and βCD **(a)**; {βCD · C_4E_2}, 1 : 1 physical mixture of βCD and C_4E_2, and βCD **(b)**; {βCD · C_6E_2}, 1 : 1 physical mixture of βCD and C_6E_2, and βCD **(c)**, all prepared at ambient humidity.

As shown above, the thermograms of all prepared compounds are qualitatively different from those of βCD and of the corresponding 1 : 1 physical mixtures, so this is a first piece of strong evidence for the formation of solid-state inclusion compounds involving the studied guests (C_4E_1, C_4E_2 and C_6E_2) and βCD (host).

Powder X-ray diffraction (PXRD)

Powder diffractograms can sometimes be used to quickly identify the type of crystal packing of cyclodextrin inclusion compounds using the concept of crystal isostructurality.[22,23] This concept applies to two or more crystalline phases that display identical or quasi-identical packing motifs. A prerequisite for isostructurality of two phases is the similarity of unit cell dimensions and of the internal arrangement of molecules. Within an isostructural series of crystalline inclusion compounds based on a particular cyclodextrin, the main features of the PXRD patterns should essentially coincide, regardless of the nature of the included guest.[23] During the formation of inclusion compounds, βCD has a tendency to form head-to-head dimers held by multiple intermolecular O–H···O hydro-

gen bonds across the βCD secondary rims. These βCD dimers appear in inclusion compounds in a variety of 3D structural arrangements, classified as "channel", "intermediate", "chessboard" or "screw-channel".[22–24]

Using the concept of isostructurality, it is possible to identify the type of crystal packing for the prepared solid-state inclusion compounds. The powder diffractogram for {βCD · C_4E_1} (2θ = 4.3, 6.0, 7.1, 9.0, 10.6, 11.6, 12.1 and 14.6) is similar to the characteristic diffractogram of inclusion compounds with cage structure (2θ = 4.2, 5.0, 7.6, 9.0, 10.8, 11.7, 12.6 and 14.6), especially at low angles (2θ between 3 and 20°). This similarity suggests that {βCD · C_4E_1} crystallizes as a monomeric complex in a cage type structure (*herring-bone* packing arrangement).

PXRD patterns for {βCD · C_4E_2} and {βCD · C_6E_2} are almost coincident, both in position and in relative intensity of the peaks (2θ = 6.0, 7.2, 9.6, 9.9, 12.1, 12.5, 13.4, 14.5, 15.1, 17.6 and 18.8), suggesting that the two inclusion compounds present the same crystalline packing arrangement and their diffractograms match with that of an isostructural series of dimeric complexes on a channel structure (2θ = 6.0, 7.3, 9.4, 9.8, 11.8, 12.6, 13.8, 14.5, 15.1, 15.6, 17.5 and 18.8; space group *C*2).[23,24]

Fig. 4 presents a set of PXRD patterns of {βCD · C_4E_1} at room temperature and defined RHs (0%, 15%, 20%, 58%, 80% and 100%). The first general observation is that the RH appreciably affects the PXRD patterns, pointing to structural changes due to variations in the hydration level of the crystalline hydrate inclusion compound. For RHs between 20% and 58%, the PXRD patterns present reflections at the same angles, with gradable intensity variations. In turn, for diffractograms at high hydration level, at RH between 80% and 100%, several additional reflections appear at low angles (2θ values $<13°$). Abrupt changes are also observed for RHs below 20%, for RHs 15% and 0%. Lacking many of the reflections observed for higher RH values, these PXRD patterns only show two sharp and intense peaks at low angles, apart from a number of uncharacteristic weak and wide features, especially for $2\theta \geq 13°$. These observations suggest an appreciable loss of crystallinity at low water contents (RHs 15% and 0%), in particular at RH 0%, thus pointing to the structural relevance of hydration water for preservation of the crystalline structure of {βCD · C_4E_1}.

Fig. 5 shows PXRD patterns of samples of {βCD · C_6E_2} at room temperature and defined RHs (0%, 15%, 20%, 58%, 80% and 100%). The powder diffraction patterns at room

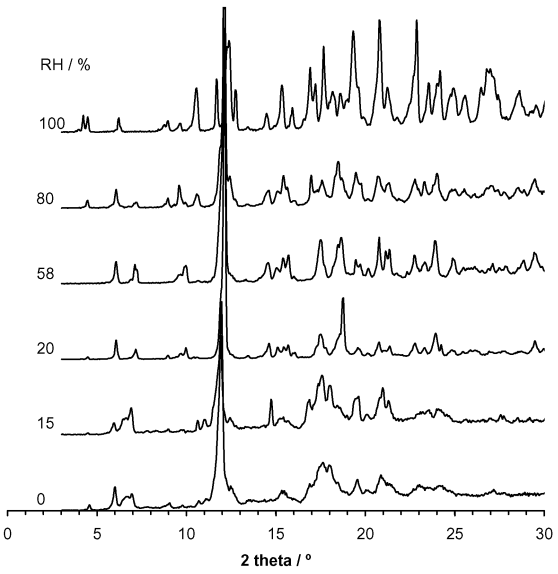

Fig. 4 PXRD patterns for samples of {βCD · C_4E_1} prepared at room temperature and at defined RHs (0%, 15%, 20%, 58%, 80% and 100%).

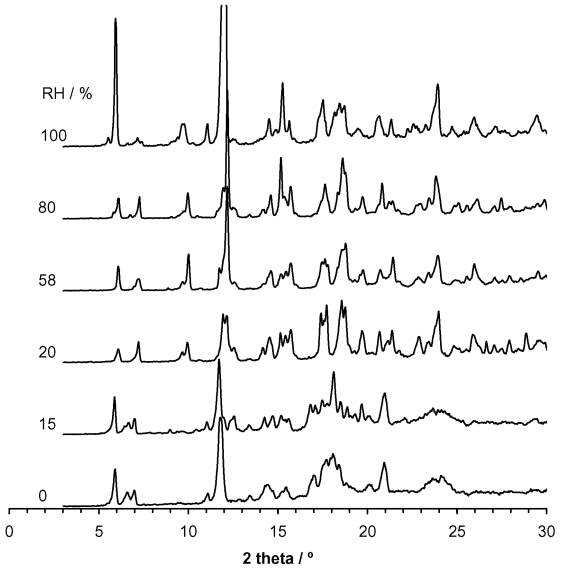

Fig. 5 PXRD patterns for samples of {βCD · C_6E_2} prepared at room temperature and at defined RHs (0%, 15%, 20%, 58%, 80% and 100%).

temperature and defined RHs for the solid-state inclusion of C_4E_2 in βCD are not presented here since they are almost the same as for {βCD · C_6E_2}. Hence, the discussion for {βCD · C_6E_2} applies also to the powder diffraction patterns of {βCD · C_4E_2}.

The first general observation from Fig. 5 is that the hydration level appreciably affects the PXRD patterns. Despite the similarity between the diffractograms at RH 0% and 15%, considerable differences are observed relative to the remaining diffractograms. However, the PXRD patterns from RH 20% to 80% present only gradual and minor alterations. In particular, only small intensity changes are observed for RH above 20%, thus suggesting that the crystalline structure of this inclusion compound is essentially preserved within this range of RHs. In turn, at RH 100%, additional reflections appear at low angles (2θ values $<13°$) and considerable changes in the relative intensity of some reflections are also observed. For RH 0% and 15%, a number of uncharacteristic weak and wide features, especially for $2\theta \geq 13°$, are observed. These diffraction features suggest an appreciable loss of crystallinity at low water contents (RHs 0% and 15%), thus stressing the structural relevance of hydration water for preservation of the crystalline structure of {βCD · C_6E_2}.

On the whole, the distinct crystal structures of {βCD · C_4E_1} (cage packing), {βCD · C_6E_2} and {βCD · C_4E_2} (both present a channel type structure) are preserved for humidities $\geq 20\%$. Below these RH values, the crystalline structures tend to collapse due to loss of hydration water, thus pointing to the importance of hydration water for preservation of the crystalline structures, and setting lower RHs for preventing structural collapse.

FT-Raman spectroscopy

Considering the solid-state inclusion compounds stoichiometry (probably 1 : 1 for all the prepared compounds) and the relative number of vibrational oscillators of the host (βCD) and guest molecules (C_4E_1, C_4E_2 and C_6E_2), the Raman spectra for {βCD · C_4E_1}, {βCD · C_4E_2} and {βCD · C_6E_2} are mostly dominated by cyclodextrin bands. While no significant differences in Raman shifts were observed upon comparison of the FT-Raman spectra of the solid-state inclusion compounds with those of the corresponding 1 : 1 physical mixtures, relevant variations were registered mainly in the relative intensities of some Raman bands. This should not surprise us,

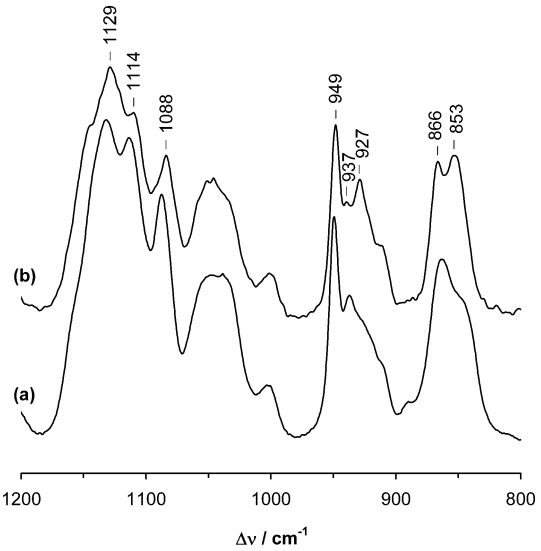

Fig. 6 FT-Raman spectra, between 1200 and 800 cm^{-1}, for samples of {βCD · C_4E_1} **(a)** and the 1 : 1 physical mixture of βCD and C_4E_1 **(b)**, at ambient humidity.

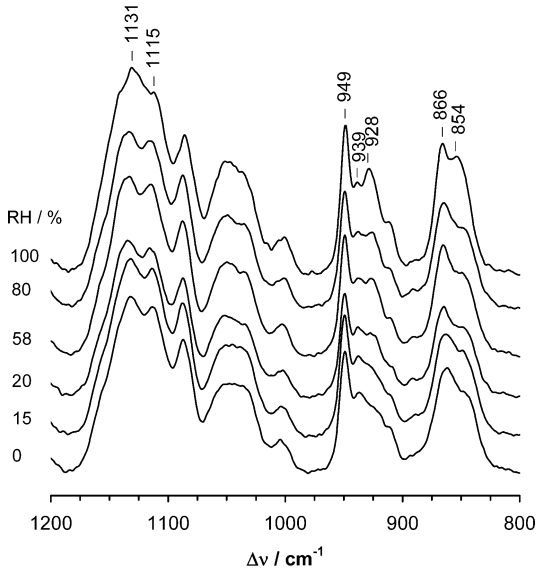

Fig. 7 FT-Raman spectra for samples of {βCD · C_4E_1} at defined RHs (0%, 15%, 20%, 58%, 80% and 100%) in the 1200–800 cm^{-1} region, at room temperature.

since vibrational Raman spectroscopy is known to be sensitive to weak non-covalent interactions that occur in the formation of inclusion compounds, like van der Waals and hydrophobic interactions, and hydrogen bonding.[25]

Fig. 6 shows the FT-Raman spectra for {βCD · C_4E_1} and the 1 : 1 physical mixture, in the 1200–800 cm^{-1} wavenumber region. The bands affected by guest encapsulation are found by comparison of spectra of {βCD · C_4E_1} and the 1 : 1 physical mixture. Those bands can be generally assigned to various C–O stretchings in βCD (bands maxima at 1129, 1114, 1088, 1048, 949, 937 and 929 cm^{-1}) and to CH_2 bendings in βCD (bands maxima at 866 and 853 cm^{-1}). Since the 949, 937 and 929 cm^{-1} Raman bands are ascribed to the C–O stretching vibrations of the α(1→4) linkages, it is expected that these bands can be affected by the relative orientations of the glucose units in the βCD macrocycle, thus sensing the presence of the guest molecule in the βCD cavity. Incidentally, it should be mentioned that a previous Raman optical activity study of βCD has found that a Raman band at around 920 cm^{-1} is sensitive to the conformations around the glycosidic linkage in the βCD macrocycle.[26] Also, the relative intensities of the bands at 866 and 853 cm^{-1}, ascribed to CH_2 bendings in βCD with *trans*-C1O5–C5C6 dihedral axes, are sensitive to guest encapsulation, as they are adjacent to the disordered primary OH groups.[19]

In the spectrum of the 1 : 1 physical mixture of βCD and C_4E_1, a pair of almost equally intense bands occurring at 866 and 853 cm^{-1} originates, in the Raman spectrum of {βCD · C_4E_1}, a prominent band at 862 cm^{-1} and a shoulder in the lower Raman shift wing of this band. In addition, three Raman bands at 949, 937 and 927 cm^{-1} in the spectrum of the 1 : 1 physical mixture give rise to a pattern of two bands at 948 and 939 cm^{-1} in the Raman spectrum of solid-state inclusion compound.

The Raman spectra for {βCD · C_4E_2} and {βCD · C_6E_2} were found to be different from the spectra of their corresponding 1 : 1 physical mixtures, with similar results to those above mentioned for the Raman spectrum of {βCD · C_4E_1}, thus suggesting that {βCD · C_4E_1}, {βCD · C_4E_2} and {βCD · C_6E_2} should be solid-state inclusion compounds.

Fig. 7 presents the Raman spectra of {βCD · C_4E_1} at room temperature and at defined RH values (0%, 15%, 58%, 80% and 100%), in the 1200–800 cm^{-1} region. The Raman spectroscopic results for {βCD · C_4E_2} and {βCD · C_6E_2} are not presented here, since they are similar to those of {βCD · C_4E_1}. Hence, the discussion and interpretation carried out for {βCD · C_4E_1} at various RHs is largely applicable to the remaining two solid-state inclusion compounds.

In the Raman spectra of {βCD · C_4E_1} (Fig. 7), the 866 cm^{-1} band keeps its higher relative intensity at all recorded RH values, whereas the 854 cm^{-1} band intensity increases with RH. In addition, in the set of the bands at 949, 939 and 928 cm^{-1}, the band at 949 cm^{-1} is still the more intense at all the considered RHs, but the Raman feature at 928 cm^{-1} increases with RH, originating a relatively prominent feature at RH 100%. The band whose maximum occurs at 928 cm^{-1} has been ascribed to the C–O stretching involved in α(1→4) linkages. Hence, their strong intensity sensitivity to RH variation comes as no surprise. Among the presented Raman bands, the last important change occurs for the pair of bands at 1131 cm^{-1} and 1115 cm^{-1}. While the relative intensities of these bands do not change from RH 0% to 80%, the intensity of the 1131 cm^{-1} band increases with respect to the intensity of the band at 1115 cm^{-1} at RH 100%.

^{13}C CP MAS NMR spectroscopy

The ^{13}C CP MAS NMR spectra of the prepared compounds ({βCD · C_4E_1}, {βCD · C_4E_2} and {βCD · C_6E_2}), at ambient humidity, are presented in our previous work.[18] The formation of these three solid-state inclusion compounds was also supported by comparison of the respective spectra with that of crystalline βCD hydrate. It is well know that the spectrum of free βCD exhibits multiple resonances for each type of carbon atom. Theses features have been mainly correlated with different torsion angles about the α(1→4) linkages and with torsion angles describing the orientation of hydroxyl angles.[27–32] On the prepared compounds ^{13}C CP MAS NMR spectra, while the centres of the multiple resonances for each type of βCD carbon atom did not present significant shift changes, the multiplicity of each signal and the dispersion of the observed chemical shifts (*i.e.*, the chemical shift range that comprises all the resonances from the same carbon atom in distinct glycosidic units) decrease, particularly for {βCD · C_4E_2} and {βCD · C_6E_2}, with respect to the βCD spectrum. These observations suggest a greater equivalence of the several carbon atoms in inclusion compounds, presumably due to the improved symmetrization of the βCD macrocycle in the inclusion compounds.

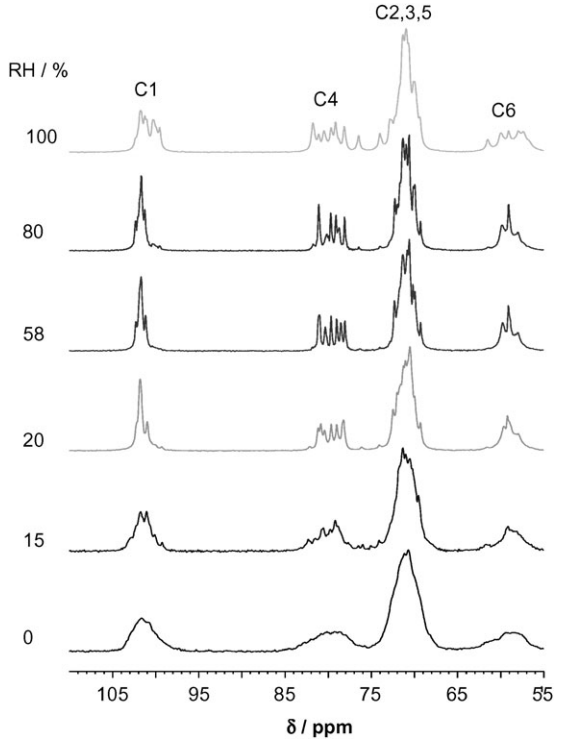

Fig. 8 ^{13}C CP MAS NMR spectra for samples of {βCD · C_4E_1} at defined RHs (0%, 15%, 20%, 58%, 80% and 100%), in the chemical shift range of the βCD carbon atoms.

The ^{13}C CP MAS NMR spectra for {βCD · C_4E_1} at defined RHs (0%, 15%, 20%, 58%, 100%), are presented in Fig. 8 in the chemical shifts range for the cyclodextrin carbon atoms. The results for {βCD · C_4E_2} and {βCD · C_6E_2} are not shown, since they are very similar to that of {βCD · C_4E_1}. The first general observation is that the ^{13}C CP MAS NMR spectra, in particular, the resonances multiplicity and the dispersion of chemical shifts for each βCD carbon atom, are affected by the hydration level. However, the centre of these multiple resonances and the signals of guest carbon atoms are not appreciably affected by the relative humidity.

At RHs 0% and 15%, the spectra present wide and uncharacteristic features very much in consonance with an amorphous solid, thus pointing to a crystalline structure collapse due to the loss of water at low hydration levels (RH < 15%). For RHs between 20% and 80% (second group), no discernible trend, either on the multiplicity of resonances or on the dispersion of chemical shifts values, is observed by varying RH. These observations suggest a global inclusion compound for these RHs. This set of spectra presents the narrowest range of chemical shifts for C1, C4 and C6 resonances, pointing to a greater symmetrization of the βCD macrocycle (each glucose unit is in a similar environment). An increase in the chemical shifts dispersion is observed for RHs 93% (not shown) and 100%, namely in carbon atoms C1, C4 and C6, suggesting a small change in the structure of the βCD macrocycle with a less symmetrical conformation relatively to the structure at RHs from 20% to 80%.

Conclusions

Solid-state inclusion compounds of small amphiphilic molecules (C_nE_m) in βCD, ({βCD · C_4E_1}, {βCD · C_4E_2} and {βCD · C_6E_2}) were successfully prepared, exhibiting interesting structural features both as inclusion compounds and crystalline hydrates. Various analytical methods (PXRD, TGA, Raman and ^{13}C CP MAS NMR spectroscopies) were used to characterize all prepared compounds, and it was shown that the prepared compounds obtained as a precipitate from aqueous solution are microcrystalline powder and true inclusion solid-state compounds. PXRD patterns suggest a *herring-bone* packing arrangement (cage structure) for {βCD · C_4E_1}. The diffraction patterns for {βCD · C_4E_2} and {βCD · C_6E_2} best match that of a channel packing compound. Both of these crystalline structures are preserved at RHs equal or above 20% and tend to loss crystallinity (collapse) at low humidities (RH < 15%) due to low hydration levels. On the whole, these observations point to the important role of hydration water in crystalline inclusion compounds, either with a cage structure or with a channel structure. Interestingly, the multiplicity of resonances and the dispersion of chemical shifts of βCD carbon atoms in the ^{13}C CP MAS NMR spectra of all the inclusion compounds exhibit a discontinuous behaviour in passing from RH 15% to 20%. At low humidities (RH 0% and 15%), single wide and uncharacteristic signals are observed suggesting amorphous solids. In turn, above RH 20%, several sharp signals present multiple resonances. These two pieces of experimental evidence seem to suggest the existence of two distinct structural phases for all the investigated solid-state inclusion compounds. The relative intensities of various Raman bands generally ascribed to C–O stretching vibrations of the βCD α(1→4) linkages (at *ca.* 949, 937 and 929 cm^{-1}), and to CH_2 bending in βCD with *trans*-C1O5–C5C6 dihedral axes (at *ca.* 866 and 853 cm^{-1}) are found to be influenced by the presence of the guest in the βCD cavity and/or by variation of ambient humidity.

On the whole, the above experiments reveal the importance of hydration water on the preservation and stabilisation of different crystalline inclusion compounds structures (cage and channel) based on amphiphilic molecules and βCD.

Acknowledgements

We are grateful to Fundação para a Ciência e Tecnologia, Ministério da Ciência e do Ensino Superior, for partial funding (SFRH/BD/1101/2000). We also thank Ms. Paula Esculcas and Dr Cláudia Morais for assistance in the solid-state NMR experiments and Dr Rosário Soares for assistance in the PDRX experiments.

References

1 W. Saenger, *Angew. Chem., Int. Ed. Engl.*, 1984, **19**, 344–362.
2 K. A. Connors, *Chem. Rev.*, 1997, **97**, 1325–1357.
3 S. J. Kitchin and T. K. Halstead, *Solid-State Nucl. Magn. Reson.*, 1996, **7**, 27–44.
4 T. Steiner and G. Koellner, *J. Am. Chem. Soc.*, 1994, **116**, 5122–5128.
5 T. Steiner, A. M. Moreira da Silva, J. J. C. Teixeira-Dias, J. Muller and W. Saenger, *Angew. Chem., Int. Ed. Engl.*, 1995, **34**, 1452–1453.
6 A. Marini, V. Berbenni, G. Bruni, V. Massarotti, P. Mustarelli and M. Villa, *J. Chem. Phys.*, 1995, **103**, 7532–7540.
7 A. M. Moreira da Silva, T. Steiner, W. Saenger, J. Empis and J. J. C. Teixeira-Dias, *Chem. Commun.*, 1996, 1871–1872.
8 A. M. Moreira da Silva, T. Steiner, W. Saenger, J. Empis and J. J. C. Teixeira-Dias, *Chem. Commun.*, 1997, 465–466.
9 K. Braesicke, T. Steiner, W. Saenger and E. W. Knapp, *J. Mol. Graphics Model.*, 2000, **18**, 143–152.
10 R. G. Winkler, S. Fioravanti, G. Ciccotti, C. Margheritis and M. Villa, *J. Comput. Aided Mol. Des.*, 2002, **14**, 659–667.
11 T. Steiner, W. Saenger, G. Keraley and R. E. Lechner, *Physica B*, 1989, **156 & 157**, 336–338.
12 T. Steiner, W. Saenger and R. E. Lechner, *Mol. Phys.*, 1991, **72**, 1211–1232.
13 J. Szejtli, *Chem. Rev.*, 1998, **98**, 1743–1753.
14 W. Saenger, J. Jacob, K. Gessler, T. Steiner, D. Hoffmann, H. Sanbe, K. Koizmi, S. M. Smith and T. Takaha, *Chem. Rev.*, 1998, **98**, 1787–1802.
15 N. J. Turro and P. C. Kuo, *Langmuir*, 1985, **1**, 170–172.
16 L. Cunha-Silva and J. J. C. Teixeira-Dias, *J. Inclusion Phenom. Macrocyclic Chem.*, 2002, **43**, 127–131.

17 T. Steiner, G. Koellner, S. Ali, D. Zakim and W. Saenger, *Biochem. Biophys. Res. Commun.*, 1992, **188**, 1060–1066.
18 L. Cunha-Silva and J. J. C. Teixeira-Dias, *J. Phys. Chem. B*, 2002, **106**, 3323–3327.
19 L. Cunha-Silva and J. J. C. Teixeira-Dias, *New J. Chem.*, 2004, **28**, 200–206.
20 F. Giordano, C. Novák and J. R. Moyano, *Thermochim. Acta*, 2001, **380**, 123–151.
21 G. Bettinetti, C. Novák and M. Sorrenti, *J. Therm. Anal. Calorim.*, 2002, **68**, 517–529.
22 Z. Metzafos, I. M. Mavridis and M. B. Hursthouse, *Acta Crystallogr. Sect. C: Cryst. Struct. Commun.*, 1996, **52**, 1220–1223.
23 M. R. Caira, *Rev. Roum. Chim.*, 2001, **46**, 371–386.
24 T. J. Brett, J. M. Alexander and J. J. Stezowski, *J. Chem. Soc., Perkin Trans. 2*, 2000, 1095–1103.
25 L. Liu and Q. X. Guo, *J. Inclusion Phenom. Macrocyclic Chem.*, 2002, **42**, 1–14.
26 A. F. Bell, L. Hecht and L. D. Barron, *Chem. Eur. J.*, 1997, **3**, 1292–1298.
27 Y. Inoue, *Ann. Rep. NMR Spectrosc.*, 1983, **27**, 59–101.
28 S. F. Tanner, S. G. Ring, M. A. Whittam and P. S. Belton, *Int. J. Biol. Macromol.*, 1987, **9**, 219–224.
29 R. P. Veregin, C. A. Fyfe, R. H. Marcelssault and M. G. Tayler, *Carbohydr. Res.*, 1987, **160**, 41–52.
30 M. J. Gidley and S. M. Bociek, *J. Am. Chem. Soc.*, 1988, **110**, 3820–3829.
31 S. J. Heyes, N. J. Clayden and C. M. Dobson, *Carbohydr. Res.*, 1992, **233**, 1–14.
32 K. Lipkowitz, *Chem. Rev.*, 1998, **98**, 1829–1873.